Ubiquinone-10 in gold-immobilized lipid membrane structures acts as a sensor for acetylcholine and other tetraalkylammonium cations.

Christoffer Mårtensson[a] and Víctor Agmo Hernández[a]*

[a]Department of Physical and Analytical Chemistry[1], Uppsala University, Uppsala, Sweden. Husargatan 3, Box 579, 75123, Uppsala, Sweden. E-mail: christoffer.workmail@gmail.com, victor.agmo@kemi.uu.se.

*Corresponding author: Phone: +46 (0) 18 471 3635. Fax: +46 (0) 18 471 3654. E- mail: victor.agmo@kemi.uu.se.

Abstract

It is reported that the reduction of ubiquinone incorporated into supported lipid bilayers and into immobilized liposome layers on gold electrodes is kinetically and thermodynamically enhanced by the presence of acetylcholine and tetrabutylammonium (TBA^+) in solution. The reduction peak and the mid-peak potentials of the redox reactions, determined by cyclic voltammetry, are displaced towards more positive potentials by approximately 500 and 250 mV, respectively, in the case of TBA^+; and by approximately 750 and 530 mV, respectively, in the case of acetylcholine. The intensity of the signal varies with the cation concentration, allowing for quantitative determinations in the millimolar range. It is proposed that the enhanced reduction of ubiquinone arises from the formation of tetraalkylammonium cation–ubiquinone radical anion ion-pairs. Electrochemical quartz crystal microbalance with dissipation monitoring (EQCM-D) measurements confirmed that the potential shift and the intensity of the redox signal are coupled with the adsorption of the tetraalkylammonium cations on the lipid membrane. The Langmuir adsorption equilibrium constant (K) of TBA^+ on lipid membranes at physiological pH is determined. In supported lipid bilayers $K = 440.7 \pm 160\ M^{-1}$, while in an immobilized liposome layer $K = 35.53 \pm 3.53\ M^{-1}$.

Keywords

Ubiquinone; tetraalkylammonium ions; ion recognition; ion quantification; supported lipid structures; acetylcholine

---

Abbreviations: UQ: ubiquinone; TBA^+: tetrabutylammonium; SLB: supported lipid bilayer; ILL: immobilized liposome layer; QCM-D: quartz crystal microbalance with dissipation monitoring; POPC: 1-palmitoyl-2-oleoyl-sn-glycero-3-phosphocholine; TMA^+: tetramethylammonium; TEA^+: tetraethylammonium; SUVs: small unilamellar vesicles; DLS: dynamic light scattering; Cryo-TEM: cryo-transmission electron microscopy; WE: working electrode; CE: counter electrode; RE: reference electrode; CV: cyclic voltammetry; CA: chronoamperometry; EIS: electrochemical impedance spectroscopy; EQCM-D: electrochemical QCM-D.

[1]Present department affiliation: Department of Chemistry-BMC, Uppsala University.

1. Introduction

Ubiquinone-10 (UQ), also known as Coenzyme Q10, is a lipid-like molecule present in most living organisms, including all animal tissues. It was first described by Crane et al. as a component of the mitochondrial respiratory chain, where it mediates electron and proton transport [1]. Apart from this function, it has been found that UQ in its reduced form (UQH_2), is a powerful antioxidant, responsible in part for the regeneration of vitamins E and C and for protecting membrane lipids against peroxidation [2-4]. In contrast, under the appropiate conditions, the oxidized and semiquinone form of UQ may act as pro-oxidants involved in the generation of the superoxide radical during mitochondrial respiration [5]. Ernster and Dallner have presented a comprehensive review on these and other aspects of the function of UQ [6]. Other studies have suggested that UQ in the cell membrane may be involved in the function of sodium pumps in *E. Coli* and *K. pneumoniae* [7; 8], although this claim has been questioned [9; 10]. Recent reports have found that UQ may be involved in redox homeostasis and act as a regulator of calcium cations in mitochondria [11]. Furthermore, studies with membrane anchored quinones have shown that these molecules can drive the transfer of divalent cations (calcium, barium, strontium and magnesium) across biomimetic membranes [12]. These examples show that UQ may be involved in other functions in living systems, besides those already well established.

The electrochemical properties of UQ have been widely studied in order to get a better insight into the mechanisms involved in its function. As the molecule is very insoluble in water, electrochemical measurements are performed either with UQ adsorbed directly on an electrode surface [13] or embedded onto supported lipid mono- and bilayers [14-20]. The latter option is preferred, as the UQ properties can then be determined in an environment similar to the one in which it is found in nature. These studies have confirmed that the reduction of UQ is a 2-electron process. The accepted redox mechanism is rather complex, as the electron transfer reactions are coupled with proton transfers from and to the surrounding media [19]. The formation of the semiubiquinone radical ($UQH^{\bullet}$) as an intermediary in most UQ redox reaction pathways has been shown [17]. The behaviour and stability of this radical and the products that can be expected from its oxidation and reduction are strongly dependent on the surrounding conditions, especially on the pH of the solution [19].

Due to its high lipophilicity and well studied electrochemical behaviour in lipophilic environments in contact with water, UQ has been used to mediate electron, proton and ion transfer reactions on electrodes modified with biomimetic membranes (examples found in references [11, 15, 21]). The obtained results have provided with a clearer picture regarding the role of UQ in cell membranes.

Furthermore, the inclusion of UQ or other electroactive substances in lipid bilayers immobilized on electrodes allows studying changes and alterations in the membrane structure upon its interaction with, for example, surfactants, as has been shown by Largueze et al. in a recent publication [22]. The inclusion of hydrophobic electroactive molecules in lipid bilayers also allows testing electrode reactions in a biomimetic environment [23-25]. The interactions of the generated redox products with the surroundings can lead to the design of sensors based on supported electroactive lipid bilayers. In this paper we have used UQ embedded in supported lipid bilayers (SLBs) and immobilized liposome layers (ILLs) on gold electrodes as a probe to recognize and quantify hydrophobic quaternary ammonium ions in solution. We studied the electrochemical behaviour of UQ embedded in lipid bilayers when these cations are present in the aqueous solution and explore the possible application of this

system as an electrochemical sensor in batch and flow conditions. It is shown that hydrophobic quaternary ammonium ions adsorbed at the water-lipid interface form ion-pairs with the semiubiquinone radial anion ($UQ^{\bullet -}$), displacing the formal potential of the system. The characterization of the produced electrochemical signal can be applied for analytical purposes. The results presented are interesting not only from the point of view of the detection and quantification of the studied ions, but also regarding the physiological implications of the effect of tetraalkylammonium ions on UQ electrochemistry.

2. Material and methods

2.1 Materials and chemicals

Dry powder of 1-palmitoyl-2-oleoyl-sn-glycero-3-phosphocholine (POPC) was from Avanti Polar Lipids (Alabaster, AL). Ubiquinone-10, sodium fluoride, acetylcholine perchlorate, lidocaine chloride, propranolol chloride, tetramethylammonium (TMA^+) fluoride, tetraethylammonium (TEA^+) fluoride and tetrabutylammonium (TBA^+) fluoride were purchased from Sigma-Aldrich (Steinheim, Germany). For experiments performed at controlled pH values, borax (100 mM, pH = 9.2) and phosphate (100 mM, pH = 7.4) buffers were employed. The pH was measured for all the prepared solutions, with no significant deviations from the established values observed. All aqueous solutions were prepared using deionized water (18.4 MΩ cm) obtained from a Milli-Q system (Millipore, Bedford, USA) and deareated 20 min with nitrogen before the electrochemical measurements. Gold coated glass slides (26x76 mm, R_{rms} < 1nm on a 1 micron scale) were supplied by Ssens (Enschede, Netherlands), cut in our laboratory to 10x26 mm pieces and stored in nitrogen atmosphere. Gold and silica coated QCM-D sensors were purchased from Q-sense (Gothenburg, Sweden).

2.2 Liposome preparation

Pure POPC and POPC:UQ 50:1 liposomes were prepared by sonication. The desired amount of POPC was weighted and dissolved in chloroform. UQ was then added from a stock solution in chloroform stored at -20 ºC. The vial containing the lipid solution was dried under a constant stream of nitrogen until a homogeneous film emerged. The vial was then left overnight in a vacuum. The lipid film was then suspended in 50 mM NaF (pH = 7.81) to obtain a final concentration of 2 mg POPC/mL. NaF was chosen as the supporting electrolyte due to the fluorides lack of surface activity on gold substrates. To obtain small unilamellar vesicles (SUVs), the lipid suspension was sonicated for 45 min in an ice-bath. Finally, the sonicated suspension was centrifuged during 10 min at 10000 rpm to remove the titanium debris produced by the sonication procedure. Characterization of the resulting liposome suspensions was performed using dynamic light scattering (DLS) and cryo-transmission electron microscopy (Cryo-TEM), confirming that SUVs are formed (Figure S-1 in the supporting information). The average radius of the obtained liposomes is 15.6 nm for pure POPC liposomes and 13.2 nm for the POPC:UQ vesicles.

2.3 Surface preparation

All gold surfaces were cleaned prior to the experiments by 40 s immersion in hot piranha solution (3:1 sulfuric acid:hydrogen peroxide). After this treatment, the surfaces were rinsed with ethanol (99% purity) for at least 1 hour, dried with nitrogen and stored in a nitrogen atmosphere. All surfaces were used within 72 hours after cleaning.

2.4 Electrochemical measurements

A customized electrochemical cell made out of polypropylene with a total volume of approximately 1 ml (Figure 1) was used for the electrochemical studies under batch conditions. Prior to use, the cell was rinsed with water and ethanol and then dried in vacuum to remove all the remaining solvent. The bottom of the cell consisted of an exchangeable gold coated glass slide, which constituted the working electrode (WE). An o-ring with a diameter of 0.6 cm was used to define the WE area. A platinum net constituted the counter electrode (CE) and an Ag|AgCl (3 M KCl, 0.21 V vs. the normal hydrogen electrode, NHE) electrode was used as the reference (RE). The electrochemical experiments were performed with an Autolab PGstat (Eco Chemie, Netherlands), an IviumStat.XR (Ivium Tehnologies, Netherlands), and an electrochemical workstation (CH Instruments, Austin, TX). No significant differences were observed between results obtained from different instruments. To form an immobilized electroactive lipid membrane layer on the surface of the working electrode, the POPC:UQ liposome suspension described in section 2.2 was added to the cell. The layer was formed upon liposome attachment to the gold surface. As will be shown in the results, this layer can consist either of an ILL or of a SLB, depending on the gold surface roughness and experimental conditions, in agreement with previous reports [26-29]. For the sake of simplicity, this layer will be termed "sensing layer", regardless of its structure. Once the sensing layer was formed, the liposome suspension was replaced with the solution to be studied, taking care not to expose the sensing layer to air. The system -before, during and after modification with the sensing layer- was characterized, and its performance tested, with cyclic voltammetry (CV), chronoamperometry (CA) and electrochemical impedance spectroscopy (EIS).

Here Fig. 1

2.5 Quartz crystal microbalance with dissipation monitoring (QCM-D)

In order to characterize the properties of the sensing layer and its interaction with the studied analites, liposome attachment and ion adsorption experiments were performed on silica and gold coated QCM-D sensors employing an E4 QCM-D instrument from Q-Sense (Gothenburg, Sweden). The QCM-D technique allows following the adhesion and adsorption of material on the sensor and provides information about the viscoelastic properties of the deposited film [30]. With this technique, the formation of the sensing layer was monitored and its properties characterized. For the performed experiments, the concentration of lipid loaded was fixed to 2 mg/mL and flow speed set to 200 µL/min. This flow rate provided with reproducible results in all the performed experiments. The temperature was set to 21 ºC. Data was simultaneously collected at the fundamental frequency of the quartz crystal (5 MHz) and at the 3^{rd}, 5^{th}, 7^{th}, 9^{th}, 11^{th} and 13^{th} overtones. The data presented in the figures correspond to the 3^{rd} overtone. For quantitative determinations, overtones 3 to 13 were taken into account.

A Q-Sense electrochemistry module (QEM 401) in conjunction with an E4 QCM-D and an Ivium CompactStat (Ivium Tehnologies, Netherlands) was employed in order to perform the electrochemical QCM-D (EQCM-D) measurements on gold coated quartz crystals. The set up of the electrochemistry module includes an Ag|AgCl RE (3 M KCl, 0.21 V vs. NHE) placed downstream and a platinum disk as CE. The WE is the gold coated quartz crystal. These experiments enabled us to follow any structural changes in the sensing layer when the redox reactions were triggered and to test the UQ electrochemistry in flow conditions. CV, CA and

EIS were employed to characterize the sensing layer and its electrochemical properties, as well as to test its application for sensing purposes.

3. Results and discussion

3.1 Formation and characterization of the sensing layer in a batch system.

By performing slow potential scans when the electroactive liposome suspension is added to the electrochemical cell, it is possible to monitor the formation of the sensing layer. It has been reported that the structure of a lipid bilayer on a gold support changes according to the applied potential [31]. Slow scan rates allow the system to reach the equilibrium structure of the immobilized lipid layers at each potential. Furthermore, it has been shown that slow scan rates are necessary to assure the complete reduction/oxidation of UQ/UQH_2 during the voltammetric cycle [18]. For these reasons, formation of the sensing layer on the gold coated glass slides was followed by performing CV at 5 mV/s. Figure 2 shows the obtained voltammograms at different times after the electroactive liposome suspension has been added. It can be seen that a characteristic signal for UQ reduction appears already in the second CV cycle at a potential of -0.38 V (vs. Ag|AgCl) (signal R1). The intensity of this signal increases continuously until the maximum surface coverage is reached. This signal is then maintained constant (CV cycle 10 onwards). It can be observed that the current arising from hydrogen evolution at the gold surface (seen at the cathodic end of the voltammogram) decreases over time as the surface is covered and blocked by the sensing layer. At faster scan rates (50 mV/s, inset in Figure 2), the intensity of R1 is enhanced and its position is shifted towards more negative potentials (to -0.475 V (vs. Ag|AgCl)). The oxidation signal is also enhanced and can be observed at -0.02 V (vs. Ag|AgCl) (signal O1). The small O1 intensity observed, as well as the large peak separation, agree with what has been observed by Jeuken et al. for tethered bilayer membranes modified with 1% UQ at pH 7.4 [15]. The low peak intensity and broad peak width of signal O1 is believed to arise from a "gating" reaction preceding the electron transfer. This reaction could be the deprotonation of the reduced form of UQ (ubiquinol (UQH_2)). The large separation between signals R1 and O1 arises from the slow charge transfer rates (both protons and electrons) at the water|membrane and membrane|electrode interfaces.

Here Fig. 2

After the sensing layer was formed, the liposome suspension in the cell was replaced by buffers of different pH values. The dependence of the position of R1 and O1 on the buffer pH and on the scan rate employed was determined in order to characterize the system. The results obtained from the analysis of the kinetics of the electrode reaction suggest a general behavior very similar to what has been reported by Moncelli et al. for a lipid monolayer containing UQ and adsorbed on a mercury electrode [18] (data not shown). It is therefore safe to assume that the present system consists of an electroactive lipid membrane structure adsorbed on the gold surface. Impedance data obtained for the system can be very well fitted to the equivalent circuit proposed in other reports for a SLB (e.g. [32]) suggesting the formation of the latter. The equivalent circuit used for fitting the experimental data is $R_s(R_mCPE1)CPE2$, where the terms within brackets are parallel. $R_s = 30 \pm 0.6\ \Omega\ cm^2$ and $R_m = 0.71 \pm 0.05\ k\Omega\ cm^2$ represent the electrolyte and the SLB resistance respectively. CPE1 is a constant phase

element found in parallel to the SLB resistance and is defined by the values P1 = 0.74 ± 0.02 and T1 = 72.1 ± 7.8 μF cm^{-2} (impedance at the CPE = $(T^*(\omega i)^P)^{-1}$, where ω is the angular frequency). CPE2 describes the capacitance of the underlying water layer, and is given by P2 = 0.73 ± 0.02 and T2 = 226 ± 4.9 μF cm^{-2}. The determined R_m is much lower than expected for a SLB (typical values between 10-10^4 kΩ cm^2), while the estimated T1 is too high (typical bilayer capacitance values 0.5-1 μF cm^{-2}). Both observations indicate that the formed SLB is not defect free. It is likely that a SLB structure is formed in flat terraces on the employed gold, while rougher areas on the surface will remain uncovered, giving rise to the recorded impedance signal. In other words, the SLB building the sensing layer is not perfect, and may present a high density of defects.

3.2 Effect of hydrophobic quaternary ammonium salts in the electrochemical signal

When the solution in the cell contains a hydrophobic quaternary ammonium ion such as TBA^+, a new redox pair (defined by the reduction and oxidation signals R2 and O2, repectively) is detected in CV, as shown in Figure 3. In experiments performed on a pure POPC sensing layer and on bare gold this signal is not observed, implying that UQ should be involved in the electrochemical reaction. Substituting TBA^+ by TMA^+ or TEA^+ does not produce the same kind of signal (data not shown). Importantly, at the two pH values studied (7.4 and 9.2), the peak height of both R2 and O2 increases with TBA^+ concentration until a limit value is reached. As seen in Figure 3, the signals obtained at pH 9.2 are better defined, and further analysis in this section will be focused on the process at that pH. It is observed that the UQ reduction signal R1 is displaced towards more positive potentials when TBA^+ is present (a phenomenon appreciated as well at pH = 7.4). This displaced reduction signal is labeled R1'. At low TBA^+ concentrations both R1 and R1' are observed, with the former completely disappearing when the TBA^+ concentration increases. The R1' peak height decreases as the TBA^+ concentration increases and its position is shifted slightly towards more positive potentials. Figure 4 shows the variations of R1' and R2 peak currents ($I_{p,r}$) with respect to the concentration of TBA^+ in the sample. The increase of R2 peak height with increasing TBA^+ concentration follows a typical Langmuir behavior, suggesting that the signal is related to the amount of TBA^+ adsorbed on the sensing layer. Different linearizations of the Langmuir isotherm gave all a good fitting to the experimental data. On the other hand, the intensity of R1' decreases with increasing TBA^+ concentration until a constant value is reached. This limit is found at the same concentration as the limit for the increase of R2. As the increase in the peak height of R2 is correlated with a decrease in R1', it is likely that both processes consume the same reagent: UQ. Given that R1' is still observed when R2 has reached the saturation conditions, it can be concluded that the limiting value for R2 is given by the saturation of the sensing layer with TBA^+.

Here Fig. 3

Here Fig. 4

By studying the dependence of R2 and O2 on the scan rate some light can be shed onto the mechanism by which these peaks arise. Figure 5 shows the R2 and O2 peak currents and scan rate normalized peak currents as functions of the scan rate. The observed behavior is very similar to what has been reported by Mirceski et al. [33] for a coupled electron-ion transfer driven by a heme-like complex in a supported thin organic layer, pointing to some similarities with the process here described. The non linear decrease on the absolute value of the scan rate normalized R2 peak current when the scan rate is increased and the trend followed by the absolute value of the peak current indicate that the compound being reduced is produced by a previous chemical reaction, i.e., the reaction follows a CE mechanism. In the case of the O2 signal, the behavior is even more complex, showing a non linear dependence of the peak current on the scan rate and a maximum in the normalized peak current plot at v = 250 mV/s. These results imply the coupling of chemical and electrochemical reactions during the anodic scan. In short, both the reduction and the oxidation signals arising when TBA^+ is added to the system are coupled to chemical reactions. As both UQ and TBA^+ are required to give rise to this signal, one can assume that these chemical reactions involve these compounds.

Here Fig. 5

Further information about the mechanism of the reaction giving rise to R2 and O2 can be obtained from a kinetic analysis similar to the one described by Moncelli et al. [18] for UQ contained in a lipid monolayer. According to this report, a plot of the dimensionless parameter $E_p*F/(RT)$ vs. ln(v) (where E_p is the peak potential, T is the temperature in K and v is the potential scan rate) should be, for all peaks, a line with a slope with an absolute value equal to $\vec{n}+\delta\alpha$, where $\vec{n}$ is the number of electrons exchanged before the rate limiting step, α is the symmetry factor for the rate determining uptake/release of one electron from/to the electrode and δ is parameter equal to 1 if the rate determining step is an electron transfer reaction, or to 0 for a chemical rate determining step. As the value of α is expected to be close to 0.5, a valid generalization would be that a slope with a natural number value (or close to it) would indicate that the rate determining step is a chemical reaction. When performing this evaluation, the obtained slope in the case of R1' is very close to -1, similar to what is obtained in the absence of TBA^+ (data not shown) and in agreement with the cited report by Moncelli et al. for the reduction of UQ in a lipid environment. The redox pair given by O2 and R2, however, present slopes with absolute values closer to 1.5. R1' is then shown to have a chemical rate-determining step, while O2 and R2 are more likely controlled by the transfer of the second electron. Remarkably, the range of linearity obtained for R1' is much wider than when TBA^+ is not present (reported in reference 18 and confirmed in our laboratory). Scan rates as high as 2 V/s provide with responses still well within a linear relationship. This implies that the reduction of UQ at this step is complete and no semiubiquinone remains even at such fast scan rates. This is clearly an effect of the presence of TBA^+ and may be related to the shift towards positive potentials that is observed when comparing R1 and R1'.

From this analysis, it is clear that TBA^+ greatly affects the mechanism and kinetics of charge transfer leading to the reduction of UQ. An analysis of the behavior of the mid-peak potentials can help discerning if the effect of TBA^+ is also associated with the thermodynamics of UQ reduction. At the studied pH (9.2) the mid-peak potential of the R1-O1 pair (without the addition of TBA^+) is -0.24 V vs. Ag|AgCl, independent of the scan rate and in close agreement with reports in the literature (e.g., reference [14]). When adding TBA^+, two

reactions are observed. The first one is defined by R1' and O1 and the second one by R2 and O2. The position of O1 cannot be clearly determined, as it overlaps with the much larger signal O2. It is therefore difficult to determine the mid-peak potential of the R1'-O1 pair. However, it is likely that the effect of TBA^+ on the UQ → UQH_2 reduction is only kinetic and that the displacement of R1' arises because of a decrease in the peak separation. The penetration of TBA^+ into the bilayer may help exposing the UQ quinone moiety and facilitate the proton transfer, although this is still a subject for study.

On the other hand, the process defined by signals R2 and O2 has a mid-peak potential between 0.02 and -0.04 V (vs. Ag|AgCl), depending on the TBA^+ concentration. Higher TBA^+ concentrations cause a slight negative shift of the signal (60 mV negative shift between 1 and 500 mM). This mid-peak potential is over 200 mV more positive than for the R1-O1 pair. This displacement of the mid-peak potential implies a thermodynamic effect of TBA^+ in the UQ redox reaction. The peak separation between the R2-O2 pair is also much smaller than for the R1-O1 pair, and, at scan rates below 250 mV/s, the signal shows complete reversibility (peak separation = 0). However, given the chemical reactions that may occur, it cannot be asured that the reaction on the anodic scan follows the same scheme as during the cathodic scan. An anodic reaction different than the cathodic one is further suggested by the fact that, at very slow scan rates (10-20 mV/s) the anodic signal O2 is found at more negative potentials than its cathodic counterpart R2.

From the above described results, we propose that the reduction of UQ in the presence of TBA^+ is facilitated by the instant formation upon reduction of an ion-pair between the semiubiquinone radical $UQ^{\bullet-}$ and the TBA^+ adsorbed on the lipid membrane, according to the mechanism given in Reaction scheme (1):

$$\text{a) } TBA^+_{(bulk)} \rightleftarrows TBA^+_{(adsorbed)}$$

$$\text{b) } UQ + TBA^+_{(adsorbed)} + e^- \rightleftarrows UQ^{\bullet-}TBA^+ \qquad \textbf{(1)}$$

$$\text{c) } UQ^{\bullet-}TBA^+ + H^+ + e^- \rightleftarrows UQH^-TBA^+$$

All reactions in Reaction scheme (1) are responsible for signal R2. The CE behavior assumed from the analysis concerning Figure 5 arises from the requirement that TBA^+ is adsorbed on the membrane (reaction a) in order to proceed with the reduction/ion-pairing reaction (reaction b). The more positive reduction and mid-peak potentials are explained by the instant formation of an ion pair upon reduction: $UQ^{\bullet-}TBA^+$. The location of this ion pair cannot be established from our experiments but it is safe to assume that it would be located either at the lipid-solution interface or within the lipid membrane. The formation of ion pairs when an ion is formed or transferred into a lipid membrane has been shown previously [34]. A negative free Gibbs energy difference upon ion pairing can be responsible for the huge shift towards more positive potentials, as shown in Appendix A in the supporting information. The actual structure of the ion-pair and the way in which TBA^+ is coupled to the $UQ^{\bullet-}$ anion radical is unclear and out of the scope of this report. However, the formation of UQ-Cation complexes has been reported before and it is therefore not unlikely that a similar process may occur in the described system [11].

The rate limiting step in Reaction scheme (1), as deduced from the discussion above, would be the simultaneous transfer of one electron and one proton to the $UQ^{\bullet-}TBA^{+}$ ion pair (reaction c in Reaction scheme (1)). The formal potential of this reaction would depend only on the redox formal potential of the ion pair and on the pH of the solution, as demonstrated in Appendix A. On the other hand, the derivation described in the Appendix shows as well that the formal potential expected for reaction b in Reaction scheme (1) depends on the amount of TBA^{+} adsorbed on the sensing layer. The small shift of signal R2 and of the mid-peak potential towards more negative potentials upon increasing TBA^{+} concentrations, however, follows a trend opposite to the one expected. This can be explained by considering that the TBA^{+} adsorbed on the membrane-solution interface will present protons with electrostatic and steric hindrances. The local pH at the membrane-solution interface could therefore be slightly higher than in the bulk solution, resulting in the small signal drift observed.

Concerning the process giving rise to signal O2, a likely mechanism based on the experimental observations is represented by Reaction scheme (2):

$$\begin{aligned} &\text{a) } UQH^{-}TBA^{+} \rightleftarrows UQH^{\bullet} + TBA^{+}_{(\text{adsorbed/bulk})} + e^{-} \\ &\text{b) } UQH^{\bullet} \rightleftarrows UQ + H^{+} + e^{-} \end{aligned} \qquad \textbf{(2)}$$

where reaction b would be the rate limiting step according to the analysis above. The TBA^{+} released from the ion pair after the first oxidation step could be found either adsorbed on the lipid membrane or expelled into the bulk. The available data do not allow defining its actual position. The formal potential for the overall reaction represented by Reaction scheme (2) will arise from two contributions: the separation of the ion pair into UQH^{-} and TBA^{+}, and the oxidation of UQH^{-} to UQ. Due to the coupled ion-pair separation step, the overall process will have a formal potential more positive than that normally observed for the UQH^{-}/UQ pair. The formal potential of the overall reaction should vary with the pH and the TBA^{+} concentration in the bulk and/or adsorbed on the sensing layer. However, as signal O2 is partially overlapped by signal O1, it is difficult to confirm such dependence. Furthermore, as R2 is proposed to arise from a different reaction pathway, it is not possible to determine the mid-peak/formal potential of the process.

3.3 POPC:UQ sensing layer in a flow system: QCM-D and EQCM-D measurements.

3.3.1 Formation and characterization of the sensing layer.

The formation of a POPC:UQ sensing layer on gold could be followed directly employing a QCM-D setup. However, it is important to notice that the gold surface of the QCM-D sensors is not as smooth as that employed in section 3.1. Previous reports have shown that liposome rupture and spreading does not occur on QCM-D gold sensors [28], leading to the formation of an ILL, in contrast to what is observed in atomically smooth gold surfaces [26, 27, 35]. EQCM-D measurements enabled following the formation of the sensing layer both by monitoring the changes in frequency and dissipation of the sensor crystal, as well as by the appearance of the UQ redox signal in CV. The results, shown in Figure 6, clearly indicate the formation of an ILL (large frequency change (-100 Hz) accompanied by a large dissipation increase (20×10^{-6})), in contrast with the SLB obtained for the batch system described in

section 3.1. The concurrent electrochemical measurements show that the formed ILL is electroactive, with the UQ|UQH_2 redox pair being clearly detected. However, the reduction current arising from hydrogen evolution is observed at more positive potentials than on smooth gold (overlapping the UQ reduction signal). This observation agrees with what is expected for the hydrogen evolution in rougher gold, where the adsorption of protons on the surface irregularities gives rise to the observed behavior [36]. All results obtained confirm the presence of a rough gold surface leading to the formation of an ILL.

Here Fig. 6

Interestingly, as shown in Figure 6, the electrochemical reduction and oxidation signals are reflected on the QCM-D sensor loading signals. The reduction of UQ (labeled "B" in the figure) and its oxidation (A), are acompanied by spikes in the frequency and dissipation responses. In the case of UQ reduction, the frequency drops slightly (6-7 Hz) and the dissipation increases marginally ($0.3\text{-}0.4\times10^{-6}$). This implies a small increase in the sensor load upon UQ reduction. It is unlikely that this increase is related to the uptake of protons to form UQH_2, as the expected change in sensed mass in such case is too small to be detectable. However, it has been suggested that when UQ is reduced to UQH_2 the ubiquinol ring locates itself near the polar head group of the phospholipids, forming hydrogen bonds with water and increasing the packing of the phospholipids [37]. The increased packing and the extra water bound to the membrane can account for the measured frequency shift. UQH_2 is also thought to span the bilayer and interact strongly with the acyl chains of the lipids, leading to tighter packing and, therefore, to an increased density [38]. Unfortunately, the UQ reduction process is overlapped by the hydrogen formation. This causes a reduction current in CV and a drop on the mass loaded on the QCM-D sensor (probably because hydrogen bubbles displace the load of water and/or lipids on the sensor surface) (C in Figure 11). This drop overlaps with the extra-loading signal, making it difficult to quantify the actual mass increase upon UQ reduction.

The QCM-D response also shows variations in the frequency and dissipation signals at potentials were no electrochemical processes are observed. It has been shown by Burgess et al. [31] that changes in potential cause changes in the structure of the lipid membrane close to the surface and in the water layer usually found in between the lipids and the gold surface. Therefore, the water content, thickness, density and viscosity of the bilayer in contact with the sensor vary constantly upon potential scanning. Although the measurements by Burgess et al. were performed employing a supported lipid bilayer, it is likely that a similar effect will be observed in an ILL in the area of close contact between the gold substrate and the lipid membrane. This assumption accounts for the observed cyclic changes in dissipation and frequency in the QCM-D response.

3.3.2 Effect of TBA^+ in the EQCM-D response

By replacing the NaF solution with a phosphate buffer and subsequently adding a TBA^+ 50 mM solution in the same buffer, the effect of the cation on the EQCM-D response is determined. Figure 7 shows that when the potential cycles in phosphate buffer are started, the loading on the sensor decreases slightly, indicating that some of the immobilized particles are dettached (probably replaced by water). When TBA^+ is added, the QCM-D frequency signal drops strongly and the dissipation increases by several units, indicating an increase in the load

on the sensor. This increase may be given by several contributions: *i*) the "bulk effect", i.e., the changes in density and viscosity of the solution due to the inclusion of TBA^+, *ii*) adsorption of TBA^+ on the ILL, and *iii*) structural changes in the ILL. To discard the possibility that the changes observed in the EQCM-D response are due to *iii*, the contribution of the bulk effect was quantified. To this end, the shifts in frequency and dissipation when a phosphate solution was replaced by 50 mM TBA^+ in buffer were determined in a bare silica sensor. The dissipation shift recorded in this experiment was very similar to that observed in Figure 7 ($\approx 8\times10^{-6}$ in the 3rd overtone), confirming that no structural changes occur in the sensing layer. The frequency shift, on the other hand, was larger when the sensing layer was present, showing that the mass load on the sensor increases (33 Hz on the ILL and 17.2 on the bare surface). This is a good indication that TBA^+ adsorbs on the ILL. Further complementary experiments showed that no difference is observed between experiments performed with POPC:UQ ILLs with and without potential cycling, suggesting that the adsorption of TBA^+ is not affected by the UQ reduction and oxidation cycles.

The decrease in oscillation frequency observed in Figure 7 is coupled with the rise of a new redox pair (equivalent to R2 and O2 in section 3.2). The potential cycles are also reflected as cyclic patterns in the QCM-D response. The general shape of these patterns is substantially different than what is observed in pure phosphate buffer (as can be seen in Figure S-2 in the Supporting Information). Remarkably, the frequency and dissipation shifts coupled to the electrochemical signal R1' (in the presence of TBA^+) are less pronounced than for signal R1 (in pure buffer). At the same time, the peak current intensity of R1' is much lower. This further suggests that the extra load observed at the potential where UQ is reduced to UQH_2 is related to the formation of the latter and the rearrangements it causes in the membrane.

Finally, the electrical properties of the sensing layer change drastically upon inclusion of TBA^+, as EIS experiments show (Figure 8). Inclusion of TBA^+ decreases the sensing layer resistance and gives rise to a new constant phase element (CPE2) – resistor (R3) unit. This new unit in the circuit arises likely from the electron tranfer reaction involving TBA^+ and UQ (R2-O2 pair), which is expected to take place at the measuring potential. The fact that this unit appears in series with the rest of the circuit suggests that two distinct layers are involved: one in which the UQ reduction is facilitated by TBA^+, and one in which no electrochemical reactions occur at the given potential. It is likely that the former layer represents the lipids in direct contact with the electrode, where the electrochemical reaction can take place. The second layer represents the bulk solution-ILL interface, where no electron transfer occurs.

Here Fig. 7

Here Fig. 8

The differences in the sensing layer structure (SLB in section 3.1 and ILL in this section) and experimental setup (batch vs. flow, respectively), give rise to some differences in the CV response. For the flow-ILL system (inset in Figure 7), O2 is more clearly detected than its cathodic counterpart (R2), in contrast to what is observed in the batch-SLB system. The actual

effect of the flow and the lipid membrane structure on the CV response is matter for future investigations.

3.4 POPC:UQ sensing layers as an electrochemical tool for the recognition and quantification of quaternary ammonium salts.

3.4.1 Quantification of TBA^+

The dependence of the intensity of signal R2 on the concentration of TBA^+ in solution implies that the described systems can be employed to quantify it in an unknown sample. It has been shown above that TBA^+ affects the electrochemistry of UQ both in SLBs and in ILLs in batch and flow modes, respectively. This effect can be extrapolated to other hydrophobic tetraalkylammonium cations, as will be shown in section 3.4.2. The evaluation of the modified SLB and ILL systems as recognition and quantification tools for TBA^+ was performed at physiological pH (7.4). The dependence of the peak height and area under the curve of signal R2 in CV on the TBA^+ concentration was monitored. The same dependence was studied for the current intensity in double step chronoamperometry. In the batch system, the CA measurements consisted on initially fixing the potential during 5 s at 0.3 V (vs. Ag|AgCl) in order to ensure complete oxidation of UQ. The potential was then stepped to -0.2 V (vs. Ag|AgCl), hold for 5 s and stepped back to 0.3 V, to allow the reactions involved in R2 and O2 to occur in both directions. In the case of the flow system, CA signals were recorded as continuous repetitions of double step cycles consisting of 5 s equilibration time at 0.4 V followed by a 200 ms pulse at -0.1 V. After the pulse, the potential was set back again to 0.4 V for 5 s (all potentials vs. Ag|AgCl). For quantitative determinations, the currents measured after the anodic potential step were considered, as they showed better reproducibility than their cathodic counterparts.

At TBA^+ concentrations below 15 mM, the selected response variables (R2 area under the curve in CV and current intensity after the anodic potential step in CA) follow almost identical trends regardless of the structure of the sensing layer and the measurement method employed. In this region, the response variable dependence on the TBA^+ concentration follows a clear Langmuir isotherm profile (data not shown), in agreement with what is shown in Figure 4 for the same reaction at pH=9.2. Table 1 shows the determined Langmuir equilibrium constants (*K*) and the calculated surface concentration of adsorbed TBA^+ at saturation ($\Gamma_{TBA^+_{MAX}}$) for this concentration range.

At higher TBA^+ concentrations, the Langmuir behaviour is still observed in the SLBs, with the saturation of the sensing layer being reached gradually. In the case of the ILL, however, the response signal continues to increase significantly with increasing [TBA^+]. At concentrations above 100 mM the slope of the response vs. [TBA^+] curve starts to decrease, indicating that the sensing layer approaches the saturation point. Fitting the data with the Langmuir equation results in a much smaller value for *K* than for the low concentration range, as seen in Table 1. This implies that the affinity of TBA^+ for the ILL decreases after a certain surface concentration of the cation has been reached. As there is not a single value of *K* that can account for the behavior in the whole concentration range, one needs to assume that the adsorption of TBA^+ on the ILL does not follow the Langmuir isotherm. It is likely that this occurs because, in the ILL, only a fraction of the total lipid membrane surface is readily available for TBA^+ adsorption from the bulk. For low TBA^+ concentrations (< 15 mM), the cation will adsorb only on the interface between the liposomes and the bulk, which is structurally similar to an SLB. However, after the initial adsorption, the TBA^+ cations will be

distributed along the whole lipid membrane surface of the liposomes, decreasing the concentration of adsorbed TBA^+ at the ILL|bulk interface, thus allowing further adsorption of the cation.

In the case of the $\Gamma_{TBA^+_{MAX}}$ values, a real, accurate value cannot be determined by the methods employed. The absolute amounts of POPC and UQ immobilized on the sensing layer can vary from one experiment to another, modifying the amount of TBA^+ molecules that can be adsorbed. Furthermore, the contribution of capacitive charging and background processes (like gold oxidation) is not known, and, therefore, not substracted from the total charge. This may lead to an overestimation of the maximum amount of $\Gamma_{TBA^+_{MAX}}$. The values presented are, therefore, apparent values, determined without considering the differences in total lipid surface area and the contribution of other processes to the recorded transferred charge. They provide, however, with a good indication of the relative amounts of TBA^+ that can adsorb on a SLB and on an ILL, the latter being approximately one order of magnitude higher, due very likely to the larger lipid surface area of ILLs compared to SLBs.

Here Table 1

The accuracy of the presented systems to determine the concentration of TBA^+ on a problem sample was tested. A test sample ($[TBA^+]$ = 1 mM at pH = 7.4) was prepared. In the case of the batch experiments, the sample was loaded into the electrochemical cell and double step chronoamperometry was performed as described above. Different volumes of a standard solution were then added to the sample and the experiment was repeated after each addition. A standard addition curve was then built by plotting the current intensities at different times (from 100 ms to 300 ms) after the oxidative potential step against the added TBA^+ concentration. Contrary to the standard addition curves employed in, e.g. polarography, the curve obtained is not linear, but follows the Langmuir isotherm, in agreement with the results presented in the preceeding paragraph and in section 3.2. The signal at x = 0 is given by the intensity of the signal of the pure sample, against which all other values can be normalized. Extrapolating the curve to y = 0, the concentration in the sample can be calculated. The curve obtained for the normalized current recorded 100 ms after the oxidative step is shown in Figure 9. The concentration estimated this way (1.06 mM) differs only ~6% from the actual concentration of the sample.

In the case of the determination of $[TBA^+]$ in the ILL system, the sample was divided in several aliquotes and different volumes of a standard solution were added to each of them. The sample and the aliquotes with increased concentration where then let to flow sequentially through the QCM-D modified sensor while performing chronoamperometry measurements as described above. Several points after the potential pulse (ranging from 50 to 250 ms) were taken and considered to build several standard addition curves. The CA cycle giving the highest current intensity for each concentration was selected for the analysis. Figure 9 shows the curve obtained from the data at 250 ms after the potential pulse. The margin given by the stantardard error is narrow (± 0.04 mM), and the average (0.98 mM) corresponds with the actual sample concentration with an error of less than 2%.

Here Fig. 9

The results show that both SLBs and ILLs modified with UQ can be employed for quantitative determinations of TBA^+ in the millimolar range in simple solutions. Rinsing the used sensor extensively with buffer, allowed recovering the sensor surface with the current intensity dependence on the TBA^+ concentration still being observed. In the flow system, however, the signal intensities were clearly decreased in a re-used sensor surface (data not shown). This observation suggests that the ILL sensing layer is deteriorated by continous flow and redox cycles.

Unfortunately, experiments have demonstrated that the inclusion of surface active counterions (such as chloride or iodide), undermine -or even destroy completely- the detection capabilities of the system. The adsorption of these anions on the sensing surface gives rise to unpredictable signals with rather erratic behaviors. This limits strongly the application of the presented method, as all surface active anions in a hypothetical sample would need to be removed prior to the measurement. However, the obtained results represent a proof of concept approach showing that it is possible to relate the intensity of signal R2 with the concentration of TBA^+. The further development of the system into a reliable sensor is a matter for future investigations.

3.4.2 Other cations: ion recognition

Once the possibility of quantifying TBA^+ employing the gold-supported POPC:UQ sensing layers was shown, other cations of greater interest were tested. Three cations with lipophilic character containing an amine-group and of interest in medicine and pharmacy were selected. These molecules were propranolol (secondary amine), lidocaine (tertiary amine) and acetylcholine (quaternary amine), all of which are positively charged at pH = 7.4. These amine ions were selected in order to investigate if the number of side groups on the amine group is a parameter to take into consideration. The experiments were conducted in the batch-SLB system with the same setup and parameters as for the experiments with TBA^+. Repeated measurements with the three cations showed that signal R2 does not arise for lidocaine and propranolol within the potential window. For acetylcholine, on the other hand, a new distinctive signal emerged on the reduction wave at a potential of 0.24 V (vs. Ag|AgCl, scan rate = 500 mV/s, signal $R2_{Ach}$). The corresponding oxidation signal ($O2_{Ach}$) appeared on the anodic wave at a potential of 0.34 V (vs. Ag|AgCl). Both $R2_{Ach}$ and $O2_{Ach}$ showed a relationship between peak height and acetylcholine concentration. However, as both signals are close to the edge of the potential window, it is difficult to accurately determine the peak heights when analyzing the data, difficulting thus the quantitative analysis of the signal and its relationship with acetylcholine concentration. Well defined peaks are only obtained at high actylcholine concentrations (> 10 mM) and when expanding the potential scan 200 mV on the anodic end (Figure 10). However, at this potential the oxidation of gold is no longer negligible. Therefore, a large background current is overimposed on the signal, difficulting quantitative estimations.

Here Fig. 10

A remarkable feature of signals R2 and $R2_{Ach}$ is that they appear at different potentials (-0.01 V and 0.24 V (vs. Ag|AgCl), at 500 mV/s, respectively), suggesting that it is possible to use CV measurements on a supported POPC:UQ sensing layer for ion recognition purposes. The mid-peak potential of the process when acetylcholine is present is also different from the one estimated for the reaction involving TBA^+ (0.30 V (vs. Ag|AgCl) for acetylcholine versus approximately 0.0 V (vs. Ag|AgCl) for TBA^+ at pH = 7.4). Unfortunately, mixtures of TBA^+ fluoride and acetylcholine perchlorate resulted in the formation of a white precipitate. This did not allow us testing the recognition capabilities of the system with a mixed sample.

Also interesting is that the arising of a new signal has only been observed with quaternary amines with at least one long (at least 4 carbons) substituting chain. Neither short chain quaternary amines (TMA^+ and TEA^+), nor secondary and tertiary amines (propranolol and lidocaine, respectively), give rise to any new redox pair. Further investigations on various cations need to be performed in order to give better insight into what properties the ions need to possess in order to generate a new detectable redox signal in the employed system.

4. Conclusions

The electrochemical behavior of UQ embedded in lipid membranes is not simple. The complexity and number of the interfaces involved, the several chemical and electrochemical reaction pathways leading from UQ to UQH_2 and viceversa, and the rather slow rate of the electron and proton transfer reactions, result in a wide set of possible behaviors, as shown in a number of publications. The system shares features with the redox driven ion transfer reactions observed on thin-film membranes [33] and three-phase junctions [39] while, at the same time, it can behave as an adsorbed system.

The presented results show that the UQ electrochemistry in lipid membranes can be affected by the presence of quaternary amine cations. Remarkably, it is shown that acetylcholine can be detected and possibly quantified employing an UQ based sensor. The development of electrochemical acetylcholine sensors is an active research field (e.g. [40, 41]), and the system here described represents a rather simple option to carry out the detection of the cation. Further research should be performed in order to develop a working acetylcholine detector and quantificator based on an immobilized lipid membrane structure. From a fundamental point of view, the effect of both UQ and tetraalkylammonium ions on the properties of lipid membranes is also a matter for future studies.

The enhancement of UQ reduction by acetylcholine may have great implications concerning the function of these molecules in living systems. It is known that acetylcholine production in brain cells decays in Alzheimer's disease patients as the illness advances [42]. At the same time, the illness is marked by oxidative damage to the brain [43, 44]. As this report shows, acetylcholine may facilitate the reduction of UQ to UQH_2, one of the main mitochondrial antioxidants and a component of novel Alzheimer treatment strategies [44,45]. Although purely speculative at the present point, our results provide with a hypothesis about a possible contribution to the oxidative damage observed in Alzheimer's disease patients. This is an example of the potential implications of the results reported here.

Acknowledgements

The authors acknowledge Biolin Scientific (Stockholm, Sweden) for providing access to the QCM-D E4 and its electrochemistry module. Teamator AB (Helsingborg, Sweden) is acknowledged for providing access to the Ivium CompactStat. We thank Prof. Anders

Hagfeldt and his research group (Department of Physical and Analytical Chemistry, Uppsala University, Uppsala, Sweden) for providing access to the other potentiostats employed. We are thankful to Jonny Eriksson (Department of Physical and Analytical Chemistry, Uppsala University, Uppsala, Sweden) for his help with the Cryo-TEM studies. We are also most thankful to Prof. Dr. Fritz Scholz (Institut für Biochemie, Universität Greifswald) for very interesting discussions concerning the interpretation of the electrochemical results. Finally, we thank Prof. Katarina Edwards (Department of Physical and Analytical Chemistry, Uppsala University, Uppsala, Sweden) for fruitful discussions and for providing the facilities to perform the experimental work.

List of references

[1] F.L. Crane, Y. Hatefi, R.L. Lester, C. Widmer, Isolation of a quinone from beef heart mitochondria, Biochim. Biophys. Acta 25 (1957) 220-221.
[2] L. Ernster. in: R. Paoletti, et al., (Ed.), Oxidative processes and antioxidants, Raven Press, New York, 1994, pp. 185-198.
[3] R. Takayanagi, K. Takeshige, S. Minakami, NADH-dependent and NADPH-dependent lipid-peroxidation in bovine heart sub-mitochrondrial particles - dependence on the rate of electron glow in the respiratory-chain and an antioxidant role of ubiquinol, Biochem. J. 192 (1980) 853-860.
[4] K. Takeshige, R. Takayanagi, S. Minakami, Lipid-peroxidation and the reduction of ADP-Fe3+ chelate by NADH-ubiquinone reductase preparation from bovine heart-mitochondria, Biochem. J. 192 (1980) 861-866.
[5] E. Cadenas, P. Hochstein, L. Ernster, Prooxidant and antioxidant functions of quinones and quinone reductases in mammalian-cells, Adv. Enzymol. RAMB 65 (1992) 97-146.
[6] L. Ernster, G. Dallner, Biochemical, physiological and medical aspects of ubiquinone function, BBA-Mol. Basis Dis. 1271 (1995) 195-204.
[7] A.C. Gemperli, P. Dimroth, J. Steuber, The respiratory complex I (NDH I) from Klebsiella pneumoniae, a sodium pump, J. Biol. Chem. 277 (2002) 33811-33817.
[8] W. Krebs, J. Steuber, A.C. Gemperli, P. Dimroth, Na+ translocation by the NADH : ubiquinone oxidoreductase (complex I) from Klebsiella pneumoniae, Mol. Microbiol. 33 (1999) 590-598.
[9] T. Friedrich, S. Stolpe, D. Schneider, B. Barquera, P. Hellwig, Ion translocation by the Escherichia coli NADH:ubiquinone oxidoreductase (complex I), Biochem. Soc. T. 33 (2005) 836-839.
[10] Y.V. Bertsova, A.V. Bogachev, The origin of the sodium-dependent NADH oxidation by the respiratory chain of Klebsiella pneumoniae, FEBS Lett. 563 (2004) 207-212.
[11] I. Bogeski, R. Gulaboski, R. Kappl, V. Mirceski, M. Stefova, J. Petreska, M. Hoth, Calcium Binding and Transport by Coenzyme Q, J. Am. Chem. Soc. 133 (2011) 9293-9303.
[12] V. Mirceski, R. Gulaboski, I. Bogeski, M. Hoth, Redox Chemistry of Ca-Transporter 2-Palmitoylhydroquinone in an Artificial Thin Organic Film Membrane, J. Phys. Chem. C 111 (2007) 6068-6076.
[13] G.J. Gordillo, D.J. Schiffrin, Redox properties of ubiquinone (UQ10) adsorbed on a mercury electrode, J. Chem. Soc. Faraday T. 90 (1994) 1913-1922.
[14] D. Marchal, W. Boireau, J.M. Laval, J. Moiroux, C. Bourdillon, An electrochemical approach of the redox behavior of water insoluble ubiquinones or plastiquinones incorporated in supported phospholipid layers, Biophys. J. 72 (1997) 2679-2687.
[15] L.J.C. Jeuken, R.J. Bushby, S.D. Evans, Proton transport into a tethered bilayer lipid membrane, Electrochem. Commun. 9 (2007) 610-614.
[16] D. Marchal, J. Pantigny, J.M. Laval, J. Moirous, C. Bourdillon, Rate constants in two dimensions of electron transfer between pyruvate oxidase, a membrane enzyme, and ubiquinone (coenzyme Q8), its water-insoluble electron carrier, Biochemistry-US 40 (2001) 1248-1256.
[17] M.R. Moncelli, L. Becucci, A. Nelson, R. Guidelli, Electrochemical modeling of electron and proton transfer to ubiquinone-10 in a self-assembled phospholipid monolayer, Biophys. J. 70 (1996) 2716-2726.
[18] M.R. Moncelli, R. Herrero, L. Becucci, R. Guidelli, Kinetics of electron and proton transfer to ubiquinone-10 and from ubiquinol-10 in a self-assembled phophatidylcholine monolayer, Biochim. Biophys. Acta 1364 (1998) 373-384.

[19] G.J. Gordillo, D.J. Schiffrin, The electrochemistry of ubiquinone-10 in a phospholipid model membrane, Faraday Discuss. 116 (2000) 89-107.
[20] J.M. Laval, M. Majda, Electrochemical investigations of the structure and electron-transfer properties of phospholipid-bilayers incorporating ubiquinone, Thin Solid Films 244 (1994) 836-840.
[21] Y. Suemori, M. Nagata, M. Kondo, S. Ishigure, T. Dewa, T. Ohtsuka, M. Nango, Phospholipid-linked quinones-mediated electron transfer on an electrode modified with lipid bilayers, Colloid. Surface. B 61 (2008) 106-112.
[22] J.-B. Largueze, K. El Kirat, S. Morandat, Preparation of an electrochemical biosensor based on lipid membranes in nanoporous alumina, Colloid. Surface. B 79 (2010) 33-40.
[23] W.W. Yao, C. Lau, Y.L. Hui, H.L. Poh, R.D. Webster, Electrode-supported biomembrane for examining electron-transfer and ion-transfer reactions of encapsulated low molecular weight biological molecules, J. Phys. Chem. C 115 (2011) 2100-2113.
[24] A. Hosseini, J.P. Collman, A. Devadoss, G.Y. Williams, C.J. Barile, T.A. Eberspacher, Ferrocene embedded in an electrode-supported hybrid lipid bilayer membrane: a model system for electrocatalysis in a biomimetic environment, Langmuir 26 (2010) 17674-17678.
[25] D. Correia-Ledo, A.A. Arnold, J. Mauzeroll, Synthesis of redox active ferrocene-modified phospholipids by transphosphatidylation reaction and chronoamperometry study of the corresponding redox sensitive liposome, J. Am. Chem. Soc. 132 (2010) 15120-15123.
[26] J. Lipkowski, Building biomimetic membrane at a gold electrode surface, Phys. Chem. Chem. Phys. 12 (2010) 13874-13887.
[27] M. Li, M. Chen, E. Sheepwash, C.L. Brosseau, H. Li, B. Pettinger, H. Gruller, J. Lipkowski, AFM studies of solid-supported lipid bilayers formed at a Au(111) electrode surface using vesicle fusion and a combination of Langmuir-Blodgett and Langmuir-Schaefer techniques, Langmuir 24 (2008) 10313-10323.
[28] C.A. Keller, B. Kasemo, Surface specific kinetics of lipid vesicle adsorption measured with a quartz crystal microbalance, Biophys. J. 75 (1998) 1397-1402.
[29] C.A. Keller, K. Glasmastar, V.P. Zhdanov, B. Kasemo, Formation of supported membranes from vesicles, Phys. Rev. Lett. 84 (2000) 5443-5446.
[30] M. Rodahl, F. Hook, C. Fredriksson, C.A. Keller, A. Krozer, P. Brzezinski, M. Voinova, B. Kasemo, Simultaneous frequency and dissipation factor QCM measurements of biomolecular adsorption and cell adhesion, Faraday Discuss. 107 (1997) 229-246.
[31] I. Burgess, M. Li, S.L. Horswell, G. Szymanski, J. Lipkowski, J. Majewski, S. Satija, Electric field-driven transformations of a supported model biological membrane- an electrochemical and neutron reflectivity study, Biophys. J. 86 (2004) 1763-1776.
[32] L.J.C. Jeuken, S.D. Connell, M. Nurnabi, J. O'Reilly, P.J.F. Henderson, S.D. Evans, R.J. Bushby, Direct electrochemical interaction between a modified gold electrode and a bacterial membrane extract, Langmuir 21 (2005) 1481-1488.
[33] V. Mirceski, T. Dzimbova, B. Sefer, G. Krakutovski, Electrochemistry of coupled electron-ion transfer of a heme-like complex in an artificial organic membrane, Bioelectrochemistry 78 (2010) 147-154.
[34] O. Shirai, Y. Yoshida, S. Kihara, T. Ohnuki, A. Uehara, H. Yamana, Ion transport across a bilayer lipid membrane facilitated by gramicidin A - effect of counter anions on the cation transport, J. Electroanal. Chem. 595 (2006) 53-59.
[35] S. Xu, G. Szymanski, J. Lipkowski, Self-assembly of phospholipid molecules at a Au(111) electrode surface, J. Am. Chem. Soc. 126 (2004) 12276-12277.
[36] M.M. Jaksic, B. Johansen, R. Tunold, Electrochemical behaviour of gold in acidic and alkaline solutions of heavy and regular water, Int. J. Hydrogen Energ. 18 (1993) 91-110.

[37] R. Fiorini, L. Ragni, S. Ambrosi, G.P. Littarru, E. Gratton, T. Hazlett, Fluorescence studies of the interactions of ubiquinol-10 with liposomes, Photochem. Photobiol. 84 (2008) 209-214.
[38] A. Ausili, A. Torrecillas, F. Aranda, A.D. Godos, S. Sánchez-Bautista, S. Corbalán-García, J.C. Gómez-Fernández, Redox state of coenzyme Q10 determines its membrane localization, J. Phys. Chem. B 112 (2008) 12696-12702.
[39] F. Scholz, S. Komorsky-Lovric, M. Lovric, A new access to Gibbs energies of transfer of ions across liquid vertical bar liquid interfaces and a new method to study electrochemical processes at well-defined three-phase junctions, Electrochem. Commun. 2 (2000) 112-118.
[40] T.V. Barkhimer, J.R. Kirchhoff, R.A. Hudson, W.S. Messer, L.M.V. Tillekeratne, Electrochemical detection of acetylcholine and choline: application to the quantitative nonradiochemical evaluation of choline transport, Anal. Bioanal. Chem. 392 (2008) 651-662.
[41] S. Wilke, R. Schurz, H.M. Wang, Amperometric ion detection in capillary zone electrophoresis by ion transfer across a liquid-liquid microinterface. Anal. Chem. 73 (2001) 1146-1154.
[42] J.A. Richter, E.K. Perry, B.E. Tomlinson, Acetylcholine and choline levels in postmortem human-brain tissue -preliminary-observations in Alzheimers-disease, Life Sci. 26 (1980) 1683-1689.
[43] T.J. Montine, M.D. Neely, J.F. Quinn, M.F. Beal, W.R. Markesbery, L.J. Roberts, J.D. Morrow, Lipid peroxidation in aging brain and Alzheimer's disease, Free Radical Bio. Med. 33 (2002) 620-626.
[44] P.H. Reddy, Mitochondrial oxidative damage in aging and Alzheimer's disease: Implications for mitochondrially targeted antioxidant therapeutics, J. Biomed. Biotechnol. 2006 (2006) 1-13.
[45] T.L. Wadsworth, J.A. Bishop, A.S. Pappu, R.L. Woltjer, J.F. Quinn, Evaluation of coenzyme Q as an antioxidant strategy for Alzheimer's disease. J. Alzheimers Dis. 14 (2008) 225-234.

List of figure legends

Figure 1: Layout of the employed electrochemical cell. The sensing layer is formed by lipid structures (either ILL or SLB) containing UQ.

Figure 2: CV (5 mV/s, 480 s/cycle) cycles 2 (solid), 5 (dashed) and 10 (dotted), illustrating the formation of an electroactive immobilized layer of POPC:UQ lipid membranes on a gold substrate. The signal remained constant afterwards. The inset shows the second cycle obtained at 50 mV/s on the same modified electrode.

Figure 3: Cyclic voltammograms (third cycle, 500 mV/s) obtained on a POPC:UQ sensing layer supported on a gold electrode at a) pH = 7.4 and b) pH = 9.2. Solid lines: only buffer, dashed lines: TBA^+ 1 mM, dashed-dotted lines: TBA^+ 25 mM, dotted lines: TBA^+ 250 mM.

Figure 4: Dependence of the absolute reduction peak current $\left|I_{p,r}\right|$ of the R1' (empty squares) and the R2 (fill squares) signals on the TBA^+ concentration. Scan rate 250 mV/s, third cycle, pH 9.2. The solid line is the fitting of the R2 values according to the Langmuir isotherm: $\left|I_{p,r}\right| = \left|I_{p,r}\right|_{max} K\left[TBA^+\right] / \left(1 + K\left[TBA^+\right]\right)$, where $\left|I_{p,r}\right|_{max}$ is the absolute reduction peak current expected at maximum TBA^+ surface coverage and K is the TBA^+ adsorption equilibrium constant. Fitting parameters values: K = 352.9 ± 51 M^{-1} and $\left|I_{p,r}\right|_{max}$ = 3 ± 0.59 µA.

Figure 5: a) Dependence on the CV scan rate (v) of the reduction peak current ($I_{p,r}$, solid squares) and scan rate normalized peak current (empty triangles) of the cathodic R2 peak arising upon addition of 500 mM TBA^+ to the POPC:UQ sensing layer b) Dependence on the CV scan rate of the oxidation peak current ($I_{p,o}$, solid squares) and scan rate normalized peak current (empty triangles) of the anodic O2 peak arising in the same system. Other experimental conditions are the same as employed in Figure 4.

Figure 6: Changes in frequency and dissipation (flow 200 µL/min, top) upon addition of POPC:UQ liposomes to a QCM-D gold sensor. The bottom curve shows the current evolution ($I(t)$ vs. t) obtained from CV (v = 5 mV/s) over the same time scale. The inset shows the actual cyclic voltammograms ($I(E)$ vs. E curves). The vertical lines point the ocurrence of the events observed in CV: A) re-oxidation of UQ, B) reduction of UQ and C) hydrogen evolution on the gold surface.

Figure 7: Changes in frequency and dissipation (flow 200 µL/min, top) upon addition of TBA^+ 50 mM (pH = 7.4) to an immobilized POPC:UQ liposome layer on a QCM-D gold sensor. The bottom curve shows the current evolution ($I(t)$ vs. t) obtained from CV (v = 150 mV/s) over the same time scale. The inset shows the actual cyclic voltammograms ($I(E)$ vs. E curves).

Figure 8: Nyquist (a) and Bode (b) plots of a gold QCM-D sensor modified with an immobilized layer of POPC:UQ liposomes in phosphate buffer (squares) and in a 50 mM TBA^+ solution in the same buffer (triangles). Open symbols in the Bode plot represent the phase behavior. Solid lines represent the fitting according to the equivalent circuits shown. EIS data measured at 0 V vs Ag|AgCl and 50 mV amplitude. Fitting parameters: In phosphate buffer: R1 = 5.3 ± 1 Ω cm^2, R2 = 433.5 ± 52 kΩ cm^2, CPE1: P = 0.92 ± 0.01, T = 9.9 ± 1 µF cm^{-2}. In TBA^+ 50 mM: R1 = 7.4 ± 2.9 Ω cm^2, R2 = 191.1 ± 49 kΩ cm^2, R3 = 184.4 ± 60 Ω

cm^2 , CPE1: P = 0.93 ± 0.06, T = 99.2 ± 17.6 µF cm^{-2}, CPE2; P = 0.87 ± 0.21, T = 22.2 ± 20.7 µF cm^{-2}.

Figure 9: Standard addition curves obtained for a TBA^+ 1 mM sample solution (pH = 7.4) on POPC:UQ sensing layers on gold. The y-axis represents the CA oxidation current normalized respect to the signal obtained with the pure sample ($I_{o\,(N)}$). The lines represents the fitting to a displaced Langmuir isotherm, given by $I_{o\,(N)} = I_{o(N)\ max} K\left(\left[TBA^+\right]_{added} + \left[TBA^+\right]_{sample}\right) \Big/ \left(1 + K\left(\left[TBA^+\right]_{added} + \left[TBA^+\right]_{sample}\right)\right)$, where $I_{o\,(N)} = I_o\left(\left[TBA^+\right]_{added}\right) \Big/ I_o\left(\left[TBA^+\right]_{added} = 0\right)$. The intercepts in the x-axis are therefore equal to $-\left[TBA^+\right]_{sample}$. Filled squares and solid line: SLB batch system (K = 308.7 ± 133). Empty circles and dashed line: ILL flow system (K = 269.2 ± 59.8).

Figure 10: Cyclic voltammograms (fifth cycle, 500 mV/s) obtained on a POPC:UQ sensing layer supported on a gold electrode at pH = 7.4 and with acetylcholine bulk concentrations 15 mM (solid line) and 25 mM (dashed line).

Tables

Table 1: Langmuir equilibrium constant *K* and saturation value $\Gamma_{TBA^+_{MAX}}$ determined electrochemically for TBA^+ adsorption at pH = 7.4 in the two different gold-supported POPC:UQ 50:1 membrane systems tested.

		SLB		ILL
		CV[a]	**CA**	**CA**
[TBA^+] < 15 mM	***K* / M^{-1}**	489.2 ± 66.5	217.1 ± 165[b]	311.5 ± 49.5[b]
	$\Gamma_{TBA^+_{MAX}}$ [c]/pmol cm^{-2}	61.6 ± 1.3	180 ± 80.0	385 ± 23.0
Whole [TBA^+] range	***K* / M^{-1}**	390.2 ± 67.6	440.7 ± 160[b]	35.53 ± 3.53[b]
	$\Gamma_{TBA^+_{MAX}}$ [c]/pmol cm^{-2}	54.8 ± 1.7	136.5 ± 22.6	635 ± 77.5

[a]800 mV/s, R2 areas under the curve were determined for the fifth cycle. [b]Average of the values calculated for all measured current intensities between 50 and 250 ms after the anodic potential step. [c]Apparent values, determined by extrapolation to the saturation conditions of the charge transferred in each measurement.

Figure 1

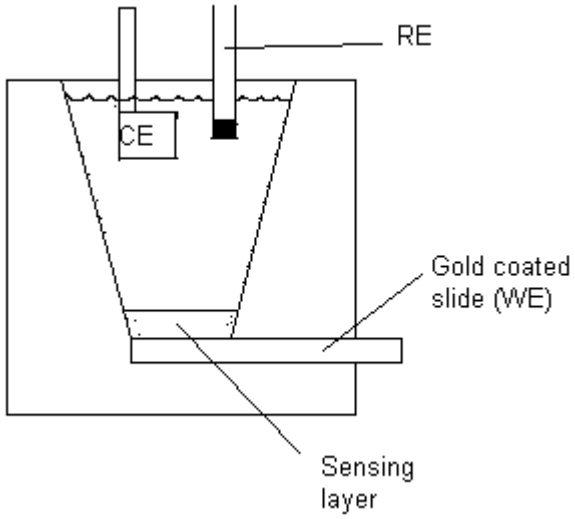

Figure 2

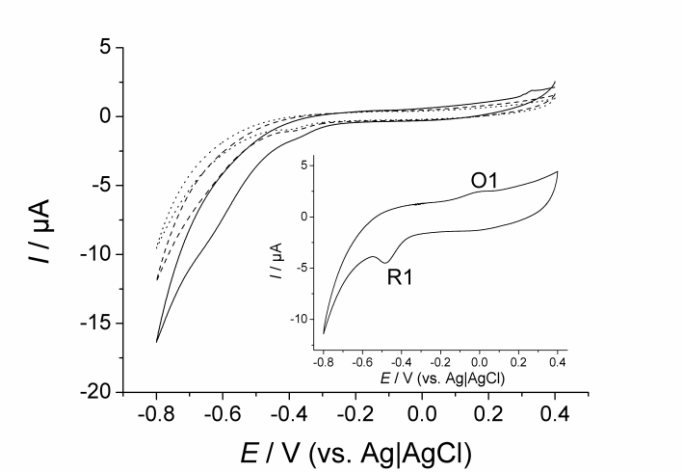

Figure 3

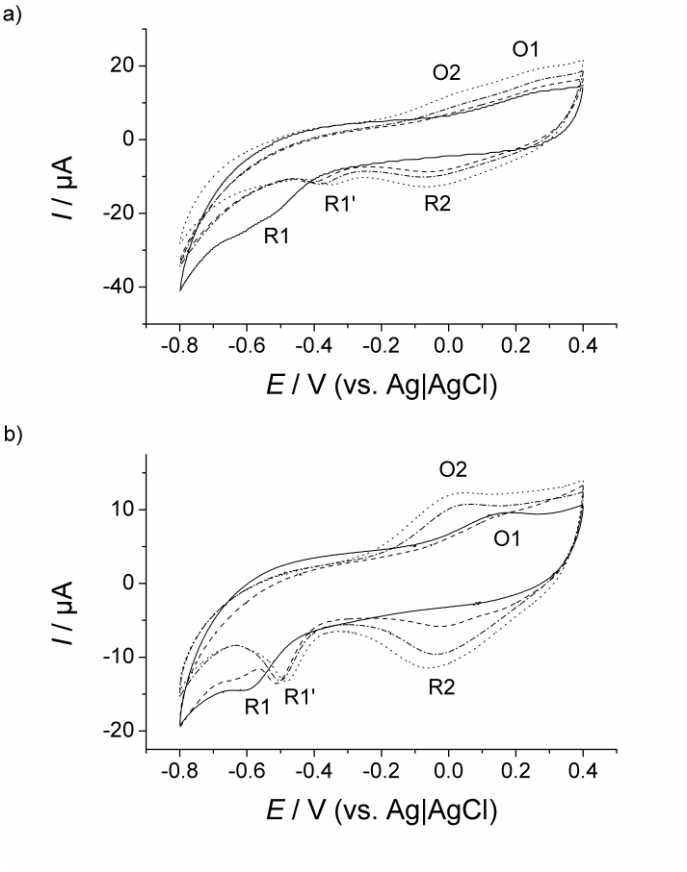
a)
20
0
-20
-40
I / µA
O1
O2
R1'
R2
R1
-0.8
-0.6
-0.4
-0.2
0.0
0.2
0.4
E / V (vs. Ag|AgCl)
b)
10
0
-10
-20
I / µA
O2
O1
R2
R1
R1'
-0.8
-0.6
-0.4
-0.2
0.0
0.2
0.4
E / V (vs. Ag|AgCl)

Figure 4

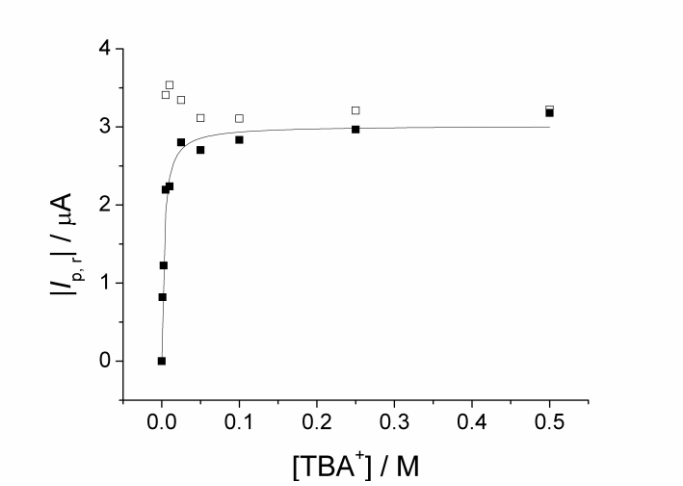

Figure 5

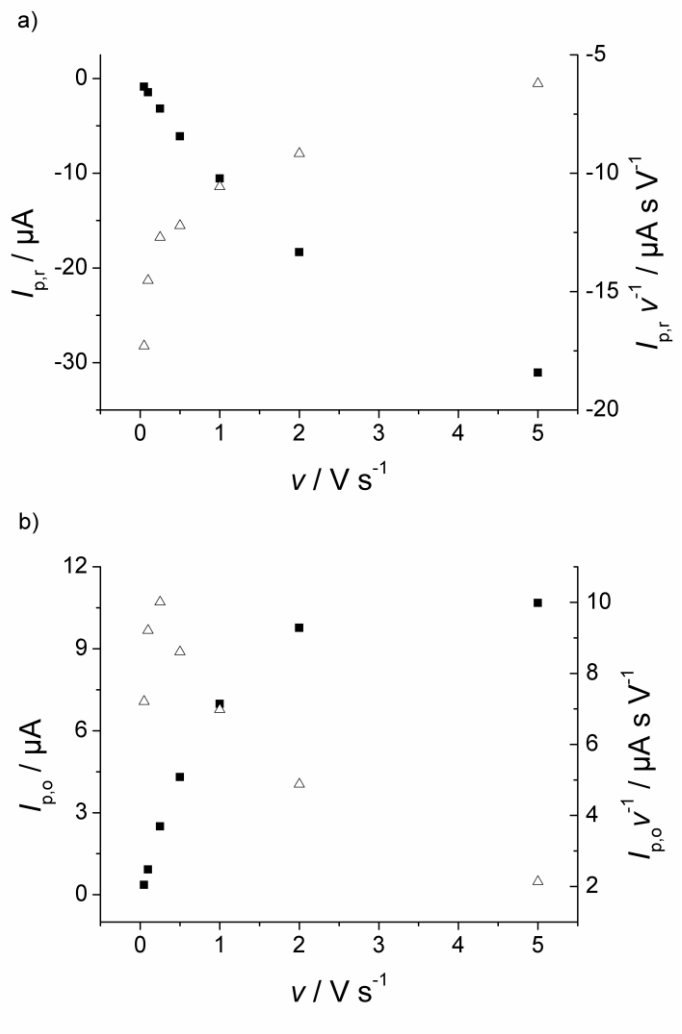
a)
0
-10
-20
-30
-5
-10
-15
-20
0
1
2
3
4
5
$I_{p,r}$ / µA
$I_{p,r} v^{-1}$ / µA s V^{-1}
v / V s^{-1}
b)
12
9
6
3
0
10
8
6
4
2
0
1
2
3
4
5
$I_{p,o}$ / µA
$I_{p,o} v^{-1}$ / µA s V^{-1}
v / V s^{-1}

Figure 6

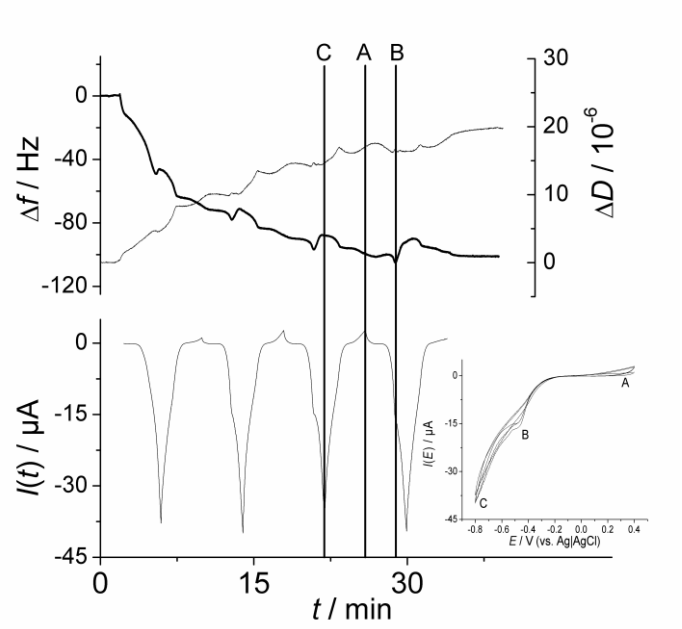
C
A
B
0
-40
-80
-120
Δf / Hz
30
20
10
0
ΔD / 10^-6
0
-15
-30
-45
I(t) / µA
0
15
30
t / min
I(E) / µA
E / V (vs. Ag|AgCl)
A
B
C

Figure 7

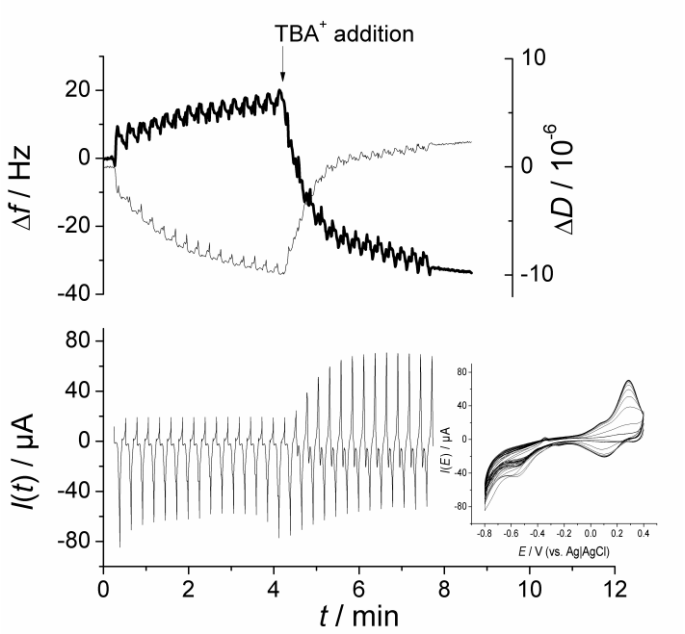

Figure 8

a)

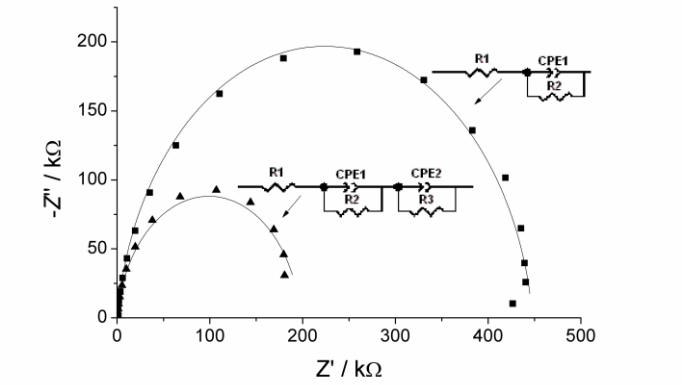

b)

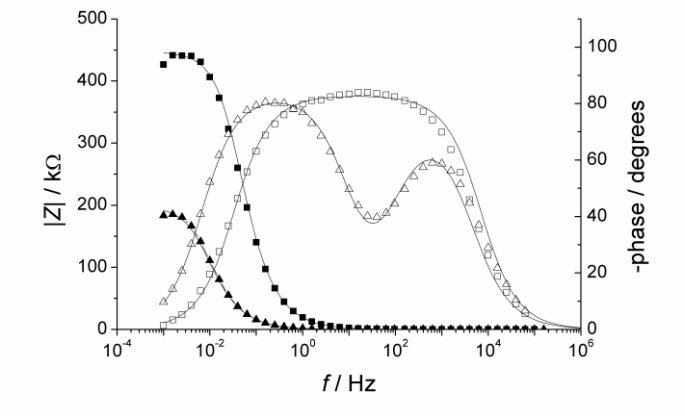

Figure 9

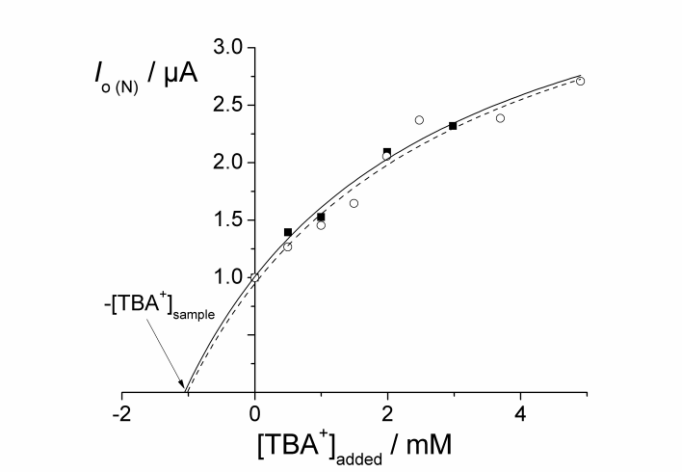

Figure 10

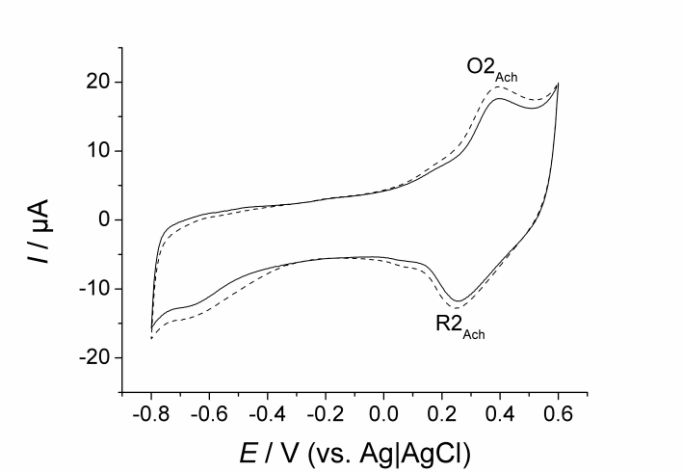

Vitae

CM started his studies in chemical engineering 2004 at Uppsala University (Uppsala, Sweden). During his studies he also obtained a double degree in economics, conducted studies at Università degli studi di Pavia (Pavia, Italy) and Universidad Complutense de Madrid (Madrid, Spain) as well as obtaining several scholarships. In 2011 he wrote his master thesis at the Department of Physical and Analytical Chemistry at Uppsala University under the supervision of Victor Agmo Hernandez and Katarina Edwards.

VAH obtained his B.Sc. in chemistry at the Instituto Tecnológico y de Estudios Superiores de Monterrey (Monterrey, Mexico). He obtained a Ph.D. in Analytical Chemistry at Greifswald University (Greifswald, Germany). Since 2008 he is a postdoc at the Department of Physical and Analytical Chemistry at Uppsala University (Uppsala, Sweden). His research is focused on fundamental properties of lipid membranes, on interfacial phenomena involving lipids and peptides and on the development of electrochemical methods to study lipid-substrate interactions.